J Mater Sci (2009) 44:5701–5712
DOI 10.1007/s10853-009-3757-4

REVIEW

Characterization of catalysts obtained from rapidly quenched alloy precursors by electrochemical/chemical processes of material degradation—selected examples

Marcin Pisarek · Maria Janik-Czachor · Tomasz Płociński · Mariusz Łukaszewski

Received: 27 May 2009 / Accepted: 15 July 2009 / Published online: 4 August 2009

Abstract Rapidly quenched amorphous alloys—containing metallic or metalloid elements—are precursors for selective catalysts of many technically important reactions. To increase their activity, various methods of material degradation occurring at the surface and in the bulk of the rapidly quenched alloys have been used for promoting the catalytic performance of such materials. The modifications of the structure, composition, and morphology of the substrate proved to be efficient in transforming inactive metal alloy precursors into active and selective catalysts for hydrogenation, and dehydrogenation of organic compounds, as well as for other processes like steam reforming of methanol. This article presents several examples of characterization of such catalysts and discusses their selectivity and activity in a connection with physical and chemical properties of their surfaces. Moreover, it is shown that scanning electron microscopy, Auger electron spectroscopy, scanning Auger microscopy, and energy dispersive spectrometry allowed the local changes occurring during the activation process to be identified and their implications for catalytic function to be considered.

M. Pisarek · M. Janik-Czachor (✉) · M. Łukaszewski
Institute of Physical Chemistry, Polish Academy of Sciences, Kasprzaka 44/52, 01-224 Warsaw, Poland
e-mail: maria@ichf.edu.pl

M. Pisarek · T. Płociński · M. Łukaszewski
Faculty of Materials Science and Engineering, Warsaw University of Technology, Wołoska 141, 02-507 Warsaw, Poland

Introduction

To meet the extreme demands of modern technology, functionalized materials with enhanced specific properties are needed. In particular, highly efficient and selective catalysts are required for many technically and ecologically important reactions. Some of the best known examples are applications in environmental chemistry [1–3], but, heterogeneous catalysts are also important in chemical industry and in fields such as energy storage and conversion [4, 5]. Typical catalysts are highly complex materials, e.g., multicomponent mixtures of oxides or combined oxide–metal systems. The chemical and structural complexity of these materials is crucial. Catalytic properties are often found to depend sensitively on structural parameters such as particle size or shape and chemical parameters such as the properties of the support or promoter materials. These relationships are useful in catalyst development as they provide a possibility of empirical optimization of structural and chemical properties of materials in order to maximize catalyst selectivity and activity with respect to the desired product.

Activity and selectivity are the most important characteristics of a heterogeneous catalyst. Since a separation of the desired chemical product from the by-products is often expensive and time-consuming, much effort is devoted to obtain highly selective catalysts. However, modification of a catalyst to achieve complete (100%) selectivity for a given chemical reaction is a very difficult task. Therefore, understanding selectivity at the atomic scale is crucial.

The heterogeneous catalysts are complex materials and, hence, it is inherently difficult to characterize them at the microscopic level. As a result, the underlying chemical reaction kinetics is still poorly understood at the microscopic level. Thus, more effort into characterization of catalysts

themselves is required from scientists dealing with surface science from the one side and with catalysis from the other. A fundamental understanding of reaction mechanisms on a heterogeneous catalyst would require a direct link between the microscopic structure and local chemistry of the catalyst on the one side and the reaction kinetics on the other [3].

Freund [3, 6] points out that for a long time, the chemical and structural complexity of catalyst materials has precluded detailed insights into chemical processes on catalyst surfaces. In the last decades, however, progress has been made toward a microscopic level understanding of reaction mechanisms and kinetics. Such progress has mainly been made possible by the development of new *well-defined model systems* and on advances in experimental technology and theory. It should be noted, however, that the properties of the catalytically active sites in many cases cannot be simulated by the simple use of stepped or defect-rich single crystals since they represent an inherent property of particles in the nanometer size scale. Therefore, it is problematic whether one can directly transfer the findings on catalytic behavior of model single-crystal systems to real catalysts under their working conditions.

During the last decades, a growing interest has been observed in the application of amorphous systems for catalytic studies [7, 8]. Nanocrystalline, microcrystalline metals/alloys, or amorphous metal alloys are known as *precursors* for a number of efficient catalysts for such important processes as hydrogenation and dehydrogenation of various organic compounds [9, 10]. These materials can be prepared by rapid quenching method [11], mechanical alloying [12], or chemical method of ultrafine metal precipitation [13]. In this review, we confine our discussion to the rapidly quenched alloy precursors.

Amorphous, microcrystalline, and nanocrystalline alloys exhibit a number of properties that are particularly attractive for catalytic applications. Their single-phase character ensures that the active sites are in uniform dispersion in a chemically homogeneous environment. They also have a high concentration of highly unsaturated sites, which could make adsorption and surface reactions energetically more favorable than on a corresponding crystalline catalyst. One may anticipate that even if rapid quenching does not always lead to full amorphization, a grain refinement is often obtained, which also provides some of the above features facilitating adsorption and promoting surface reactions. Therefore, amorphous alloys seem to be particularly interesting materials for catalytic studies.

It should be stressed that as far as the structure is concerned, the disordered metal alloys seem to better simulate the real metal catalysts than the small metal crystals usually used as model systems. Moreover, being structurally close to the actual active and selective catalysts, the disordered alloys offer a possibility to study the chemical effects without an interference of the structural ones. One of the effects, which may be avoided in disordered alloys' surfaces, is a modification of the surface of the substrate metal due to adsorption [14, 15] accompanied by deformation in the adsorbate molecules. Those effects, well visible by atomic force microscopy (AFM) on highly ordered metal substrates [14], may be smaller or negligible on the disordered ones, since the adsorbed molecules are apparently able to find their more suitable positions for adsorption—as the enhanced selectivity of these catalysts suggests, thus not requiring any strong deformation or modification/reconstruction of both "partners".

Further enhancement of catalytic activity and selectivity can be achieved by appropriate chemical or electrochemical modification of the catalysts precursors. In particular, various processes of material degradation, like aging in air, charging with hydrogen (from gas phase or electrochemically), or selective metal leaching may be utilized for transforming the precursors into active and selective catalysts [13, 16–19].

Developing such catalysts from composition-controlled amorphous alloys by exploiting mechanical, electrochemical, and chemical activation, calls for both fundamental and applied research. Consequently, it is important to possess means and measures of monitoring their chemical reactivity, durability, and selectivity for catalytic processes together with changes occurring at the surfaces. In all cases, the surface state of the material plays a crucial role. Thus, high-resolution methods of surface characterization, like Auger electron spectroscopy (AES) or scanning Auger microscopy (SAM) are needed to identify the factors responsible for the unique properties of such materials.

Discussion of selected examples

Steam reforming of methanol

Steam reforming of methanol is attractive for hydrogen production since it proceeds at lower temperatures than methane steam reforming. Moreover, it is an endothermic reaction [18].

Takahashi et al. [20] were able to successfully obtain catalysts for the selective steam reforming of methanol. There are two parallel reactions possible with methanol, which may simultaneously occur on a metal catalyst surface [20–23]:

$$CH_3OH \rightarrow CO + 2H_2 \text{ (decomposition)}, \quad (1)$$

$$CH_3OH + H_2O \rightarrow CO_2 + 3H_2 \text{ (steam reforming)}. \quad (2)$$

As the latter reaction 2 may produce more hydrogen from the same amount of CH_3OH than the former reaction 1, an

attempt was made to develop a selective catalyst for reaction 2.

Catalysts prepared from amorphous alloy precursors $Cu_{50}Zr_{50}$, $(Cu_{50}Zr_{50})_{100-x}Au_x$, and $(Cu_{50}Zr_{50})_{100-x}Pd_x$ by special activation procedure were used. The pretreatment included:

- prolonged annealing in air below crystallization temperature to oxidize Zr,
- reduction in hydrogen resulting in catalysts with metal on ZrO_2 support,
- several steam reforming runs.

The above three steps of activation were denoted as "regeneration runs" and were also used to improve activity when a prolonged conversion was needed.

After such a procedure with $(Cu_{50}Zr_{50})_{90}Au_{10}$ XRD revealed the following phases: Cu, Cu_2O, Au, AuO, and monoclinic ZrO_2 [20]. However, Raman investigations of steam reforming of methanol on Cu metal at temperatures varying from 343 up to 695 K have shown that CuO rather than Cu_2O is present at the surface of the working catalysts at higher temperatures [24].

The authors claim that the surface area grew from 4 up to 45 m^2/g after 6 regeneration runs. It also moderately increased from 38 up to 53 m^2/g with the Au content growing from 0 up to 53 at.% [20]. Moreover, the production of monoclinic ZrO_2 was responsible for the increase in the surface area since, apparently, Cu and Au catalyst on a support (ZrO_2) was formed. Microscopic and surface analytical data are not reported, however. Such data could be useful for a better understanding of the reaction mechanism. While reaction 1 is simple, reaction 2 requires an adequate population of ensemble entities of appropriate size, necessary for the formation of multiple adsorption species leading to the desired product. Nevertheless, with such catalysts an *excellent selectivity of 100% for the reaction* 2 was achieved, see Fig. 1.

Figure 1 shows the relationship between methanol conversion, carbon dioxide selectivity, and contact time (*W/F*) in kg s mol^{-1} over $(Cu_{50}Zr_{50})_{90}Au_{10}$ and $(Cu_{50}Zr_{50})_{90}Pd_{10}$ alloys. The conversion increased with *W/F* on both alloys, whereas the selectivity on both catalysts was almost constant over the contact time. These results suggest that carbon monoxide and carbon dioxide were produced by parallel reactions, that is, Cu–Zr–Au alloy only accelerates the reaction to carbon dioxide (2), whereas Cu–Zr–Pd alloy accelerates two reactions: transformations to both carbon dioxide (2) and carbon monoxide (1). The authors suggest that, palladium was effective for the dehydrogenation of methanol, but it was not effective for the hydrogenation of carbon monoxide. It was thus stated that the amorphous alloy containing palladium was not suitable for the steam reforming of methanol. On the basis of their catalytic

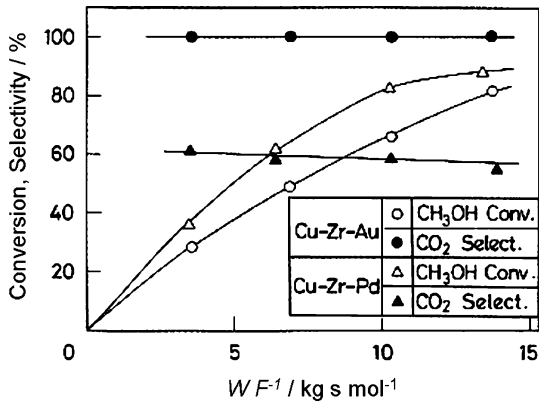

Fig. 1 Effect of contact time (*W/F*) on methanol conversion and carbon dioxide selectivity (reaction 2) over Cu–Zr–Au and Cu–Zr–Pd alloys. Data reproduced from [20]

measurements the authors concluded that the effect of gold in Cu–Zr alloy was only to increase dispersion of Cu effective for steam reforming. Any estimation of the dispersion, however, was not reported.

Hexanedinitrile hydrogenation

Deng and co-authors [13, 25, 26] developed a highly selective catalyst for the hydrogenation of organic compounds with different unsaturated functional groups. A precursor for the catalyst was Ni–Al–P amorphous alloy obtained by rapid quenching, which then was followed by alkali leaching to obtain a skeletal structure of Raney-like catalyst [22, 23].

Hydrogenation of hexanedinitrile to 1,6-hexanediamine was used as a test reaction, because of its importance for nylon production. Table 1 summarizes characteristic parameters for the new catalyst together with data for Ni–P catalyst and Raney Ni—used as a reference. It is interesting that both Ni–P and Raney-type R–Ni–P catalysts exhibit a better selectivity than the Raney Ni. Their activity calculated per H-active surface area (S_{Ni}) is also superior, as one can see from the values presented in Table 2.

The specific activities (catalytic activity per active surface area) and the TOF (turn-over factor) values observed on R–Ni–P are almost the same as those found for Ni–P catalyst. In contrast, hydrogenation activities of R–Ni–P amorphous catalyst per weight of Ni are higher than those of the Ni–P catalyst. This difference could be understood in

Table 1 Results of BET (S_{BET}) and H_2 adsorption (S_{Ni}) surface area measurements

Catalysts	Composition (at.%)	S_{BET} (m^2/g)	S_{Ni} (m^2/g Ni)
R–Ni–P	$Ni_{68}Al_{25}P_7$	87	38
Ni–P	$Ni_{88}P_{12}$	1.2	0.8
Raney Ni	$Ni_{68}Al_{32}$	106	43

Table 2 Selective hydrogenation of hexanedinitrile to 1,6-hexanediamine

Catalysts	Activity (mmol/h m^2 Ni)	Selectivity (%)	TOF (s^{-1})
R–Ni–P	42.6	70	0.10
Ni–P	36.4	75	0.090
Raney Ni	24.1	40	0.033

terms of the increase in the total surface area (S_{BET}) and the active surface area S_{Ni} due to the skeletal structure and large pore volume existing in R–Ni–P catalyst. The similar selectivities of R–Ni–P and Ni–P are mainly ascribed to the same structures of the two catalysts (amorphous structures). The residual Al, which was usually considered as both chemical and structural promoter in Raney Ni, had very little or no effect on the specific activity and selectivity of R–Ni–P catalyst in comparison with the regular Ni–P without Al. However, the high dispersion of the Ni–P alloy powders and the presence of residual Al in R–Ni–P significantly improved the thermal stability of the Ni–P amorphous structure in which the crystallization temperature increased about 80 K, as determined by DSC measurements.

The data show that R–Ni–P exhibits distinctly higher activity and about 40% higher selectivity then Raney Ni. Certainly, the lower activity of Ni–P as compared to that of R–Ni–P is a result of its low specific surface area (see Table 1). However, selectivity and TOF values for R–Ni–P and Ni–P are almost the same pointing to the role of *amorphous structure* and *the effect of P on selectivity*. X-ray photoelectron spectroscopy (XPS) data presented by the authors [13, 25, 26] suggest that, in comparison with pure Ni metal and red P, a partial electron transfer from Ni to P occurs in P-containing amorphous Ni alloys, thus making Ni electron-deficient. The latter is claimed to be favorable for adsorption of hydrogen and for the hydrogenation of organic compounds on the R–Ni–P surface containing suitable arrangement of Ni active sites. However, this electronic effect was not confirmed in other articles [27, 28].

Due to similar surface areas of the R–Ni–P and Raney Ni catalysts, as shown in Table 1, the higher activity of R–Ni–P suggested a promoting effect of amorphous structure on the catalytic activity, which resulted in the higher activity per Ni atom, i.e., higher TOF value. According to the data and the radial distribution function (RDF) curves evaluated from EXAFS spectra [11], the main reasons for the higher hydrogenation activity and TOF values as well as for the better selectivity of the as-prepared R–Ni–P amorphous catalyst as compared to the Raney Ni catalyst are as follows: the electron deficiency of Ni atoms caused by the electron transfer from Ni to P, the homogenous distribution of active sites, and the highly unsaturated active centers (offering unsaturated dangling bonds for adsorption) in R–Ni–P. Detailed results are reported elsewhere [13, 25, 26]. However, the above interpretation seems doubtful, since the authors do not confirm it in their other articles [27, 28]. A more detailed examination of local chemistry and morphology at a high lateral resolution may bring some new insight into the catalytic behavior of these skeletal systems.

Hydrogenation of pentynes

Selective hydrogenation of alkynes, called catalytic hydrorefining, is important for the petrochemical and polymer industry [29]. Although a lot of attention has been devoted to study hydrogenation of acetylene, the hydrogenation of the higher homologs is not well known. Therefore, the catalytic hydrogenation of 1 and 2 pentynes was studied to learn about the effect of the terminal and internal triple bond, and on the competitive hydrogenation of the pentyne isomers.

Hydrogenation of pentynes was investigated in the gas phase on PdZr and PdCuZr catalyst fabricated from amorphous ribbon precursors [30]. Amorphous $Pd_{25}Zr_{75}$ and $Pd_{22}Cu_{10}Zr_{68}$ ribbons were prepared by a melt quenching method in Ar atmosphere. Degradation process in dilute HF was used to remove the inactive surface oxide film from the amorphous ribbons, and to activate the catalyst precursors [30, 31]. The controlled degradation treatment resulted in 2% (PdZr) and 4% (PdCuZr) weight losses and in a porous, Raney-type surface by dissolution of Zr and removal of the inhibiting surface oxide layer. Energy dispersive spectrometry (EDS) investigations with a lateral resolution of 1 μm and a depth information of ~1 μm have shown that distribution of Pd on the surface of HF-treated PdZr catalyst remains fully homogenous. In contrast substantial inhomogeneities in the distribution of Pd and Cu within the 1-μm thick surface layer were found in HF-treated PdCuZr catalyst, see Fig. 2.

Results of selectivity measurements versus temperature are given in Fig. 3. Initial selectivity values depend on both the catalyst and the substrate and decrease with increasing hydrogen pressure and temperature in all cases except for 2-pentyne over PdCuZr. PdCuZr is completely selective in the hydrogenation of 2-pentyne: no pentane is detected and isomeric 2-pentenes are exclusively produced at any temperature and any 2-pentyne/hydrogen ratio at the beginning of the reaction:

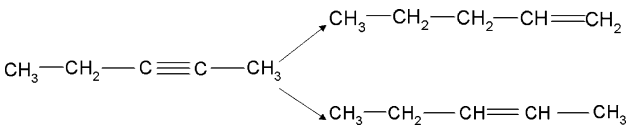

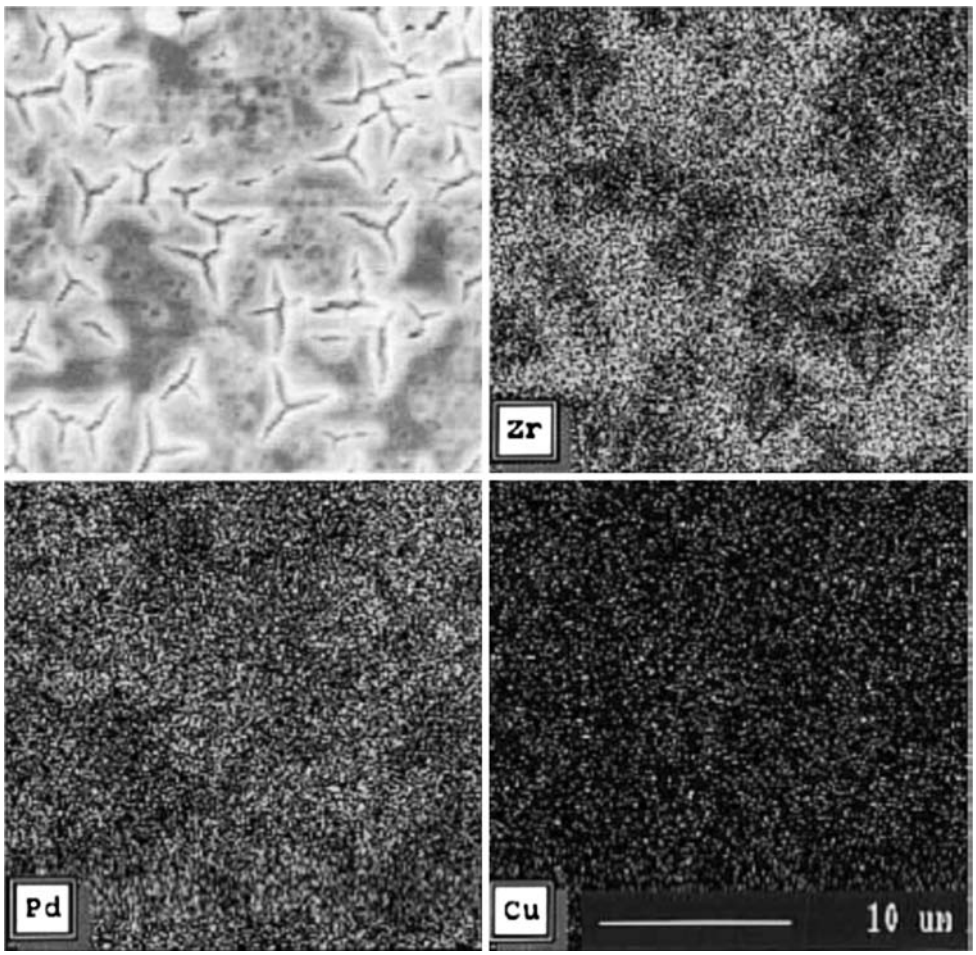

Fig. 2 X-ray electron microprobe images of the Zr (Lα), Pd (Lα), and Cu (Lα) in Pd22Cu10Zr68 alloy ribbon after HF treatment. SEM image—*upper left*. Data reproduced from [30]

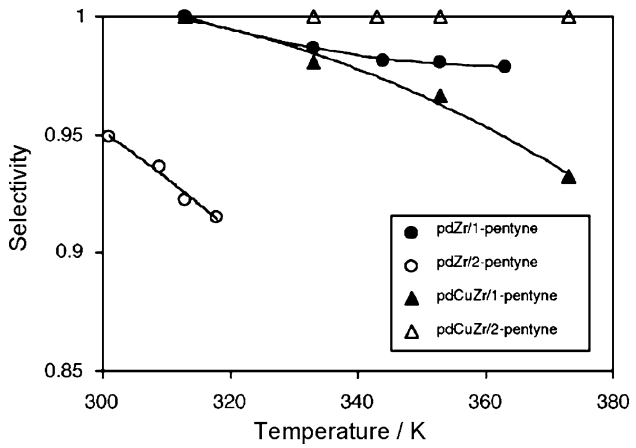

Fig. 3 The change in alkene selectivity in the hydrogenation of isomeric pentynes as a function of temperature. Data reproduced from [30]

In sharp contrast, 2-pentyne undergoes non-selective hydrogenation on PdZr yielding pentane and isomeric pentenes. The semi-hydrogenation selectivities are similar for both catalysts in the hydrogenation of 1-pentyne: selectivity values are almost always higher than 0.95 in the temperature and hydrogen partial pressure range studied. The selectivities of 1-pentyne do not change significantly when PdCuZr is used instead of PdZr. In sharp contrast, the selectivity of the hydrogenation of 2-pentyne is dramatically improved over PdCuZr. As a result, the selectivities in the hydrogenation of the two pentyne isomers are rather similar on this catalyst. In agreement with other studies [32], no change in the electronic properties of palladium was found by the addition of copper in this case. The Pd $3d_{5/2}$ line in the samples investigated is found in the range 334.5–336.0 eV. Considering the relatively low intensity of this line and the uncertainty of determining of its position due to overlapping with Zr 3d lines, the values show a good agreement with literature values for metallic Pd (335.1–335.5 eV). The increased selectivity, therefore, was attributed to the decrease in the number of ensembles of a certain size needed for multiple adsorbed (alkylidene) species, which would lead to the formation of the saturated product [32]. As activity data indicated [30, 31], PdCuZr is a less active catalyst: both pentynes react more slowly. This change, as discussed above, is brought about by dilution of the active sites and selective blocking. On the basis of these observations and the rather similar

selectivities, it is a highly probable conclusion that the difference of the adsorption ability of the two reactants disappears over PdCuZr.

A significant increase in selectivity observed in the hydrogenation of 2-pentyne over PdCuZr is attributed to an ensemble size effect: the population of ensembles of appropriate size, necessary for the formation of multiple adsorbed species leading to the saturated product, decreases by the addition of copper. Heterogeneous distribution of element components (see Fig. 2) of the catalyst may promote a suitable arrangement of active sites and a reduction of a number of ensembles of a certain size needed for multiple adsorption of pentynes.

Hydrogenation of isophorone on modified Raney Ni–Cr(Co) catalysts

Catalytic hydrogenation of α,β-unsaturated carbonyl compounds is a process of high practical potential [33–35]. Hydrogenation of the carbonyl group leads to the formation of unsaturated alcohols, hydrogenation of the C=C bond gives saturated carbonyl compounds, whereas hydrogenation of both the double bond and carbonyl group leads to saturated alcohols. An example is isophorone (3,5,5-trimethyl-2-cyclohexen-1-one) hydrogenation, which leads, among other products, to the important product of dihydroisophorone (3,3,5-trimethylcyclohexanone) that is used as a solvent for vinyl resins, lacquers, varnishes, paints, and other coatings. Since the boiling points of these products are close to one another, their separation by distillation is difficult and expensive. Therefore, the main goal for the chemists is to obtain a high catalytic selectivity for a given, expected product.

Figure 4 presents the results of catalytic tests of isophorone hydrogenation performed on Ni-based catalysts modified by doping with Cr or Co and by alkali leaching in 1 M NaOH. It is shown that while the maximum conversion in isophorone hydrogenation generally decreases with Cr or Co doping of Raney Ni catalyst, the selectivity to dihydroisophorone is considerably improved (except $NiAlCo_1$ at 80 °C). It is worth noting that Al is an electronegative metal and so the leaching process is accompanied by hydrogen evolution. This may also affect catalytic activity of the Raney-type materials.

While for Raney Ni, the selectivity rapidly drops with temperature from above 95% at 20 °C to below 30% at 80 °C, for *Cr- and Co- containing catalysts the selectivity reaches almost 100%* at room temperature and remains relatively high (above 70%) even at elevated temperature. The results show that the C=C bond can be selectively hydrogenated on the catalyst materials studied already at room temperature and under atmospheric pressure. $NiAlCr_3$ catalyst is evidently more selective than $NiAlCo_3$

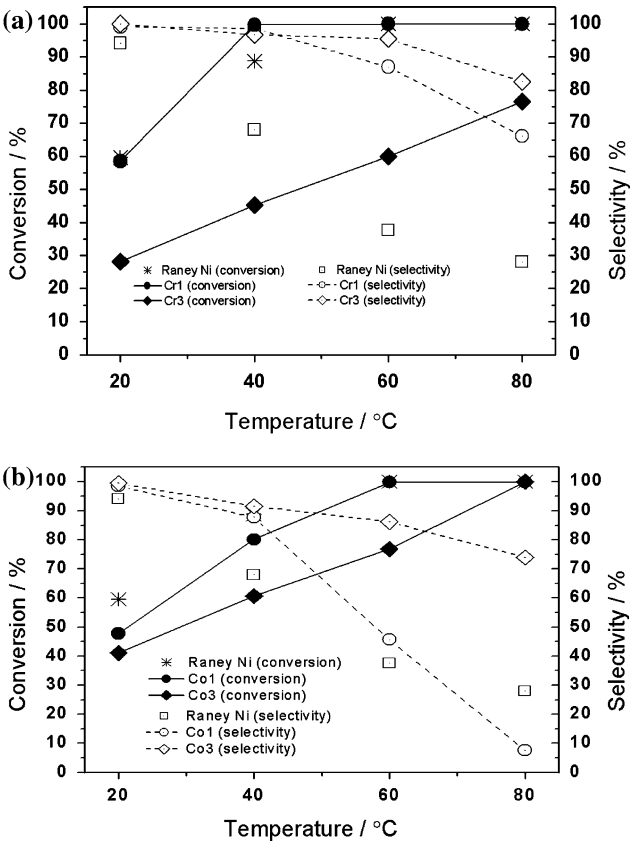

Fig. 4 Influence of temperature on total conversion and selectivity to dihydroisophorone in the hydrogenation of isophorone on Ni–Al–Cr (**a**) and Ni–Al–Co (**b**) catalysts

and its selectivity deteriorates with temperature more slowly. At elevated temperature, both these catalysts are distinctly more attractive than Raney Ni, combining high conversion with still significant selectivity.

It is noteworthy that we failed to further hydrogenate dihydroisophorone to homomentol on NiAlCr and NiAlCo catalysts. At 40 °C and $p = 70$ atm, the C=O bond is not hydrogenated even after 7 days. On the contrary, the same reaction reaches conversion level of 99% when performed on the conventional reference Al–Ni Raney catalyst. This result suggests that Co and Cr deactivate the Al–Ni catalyst for the reaction of dihydroisophorone hydrogenation and thus make it selective for hydrogenation of isophorone to dihydroisophorone only [36].

To examine the influence of the morphology and surface composition of NiAlCr and NiAlCo catalysts on their catalytic properties, high-resolution microscopic and surface analytical spectroscopic methods were applied. To examine the morphology of the working catalyst produced by leaching, the skeletal material obtained after full leaching was analyzed.

Scanning electron microscopy (SEM) images in Fig. 5 show typical morphology of the $AlNiCr_3$ catalyst after

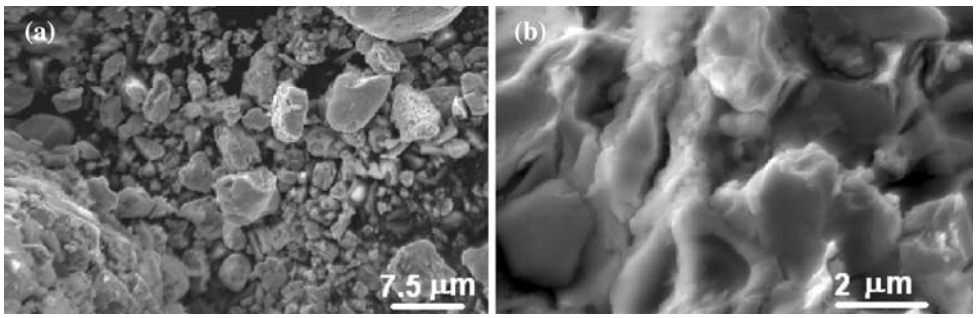

Fig. 5 Typical SEM images of Ni–Al–Cr_3 catalyst after full leaching

full leaching. Local Auger analysis including line analysis reveals that the particles at the surface contain Ni, Al, and Cr at various proportions. The results of AES local analysis along marked line presented in Fig. 6 demonstrate the above-mentioned non-uniform distribution of elements (Ni, Cr, Al) on the surface. This confirms the considerable compositional differences on the surface of the catalyst at different locations. There are domains with no Cr detectable (P10) and the others where the concentration of Cr attains ~14 at.% (P7).

Our EDS results for NiAlCr catalyst confirmed the local bulk enrichment with Cr. This technique provides the information from a volume of ca. 1 μm^3 with lateral resolution of ~1 μm. The EDS results show (see Fig. 7 and Table 3) that the average concentration of Cr in a fully leached $NiAlCr_3$ alloy may change from place to place in a range from about 1 to 6.8 at.%. These results imply that even large particles are affected by the leaching process, thus changing the bulk composition of the alloy locally.

It should be added that no simple correlation has been found between the selectivity and the BET surface area and porosity of the catalysts. In contrast, there is a positive correlation between the conversion to dihydroisophorone and the average pore diameter, see Fig. 8. Evidently, the large pores are beneficial for the catalytic activity. Therefore, one can conclude that the surface chemical effects (including those within pores) rather than the specific

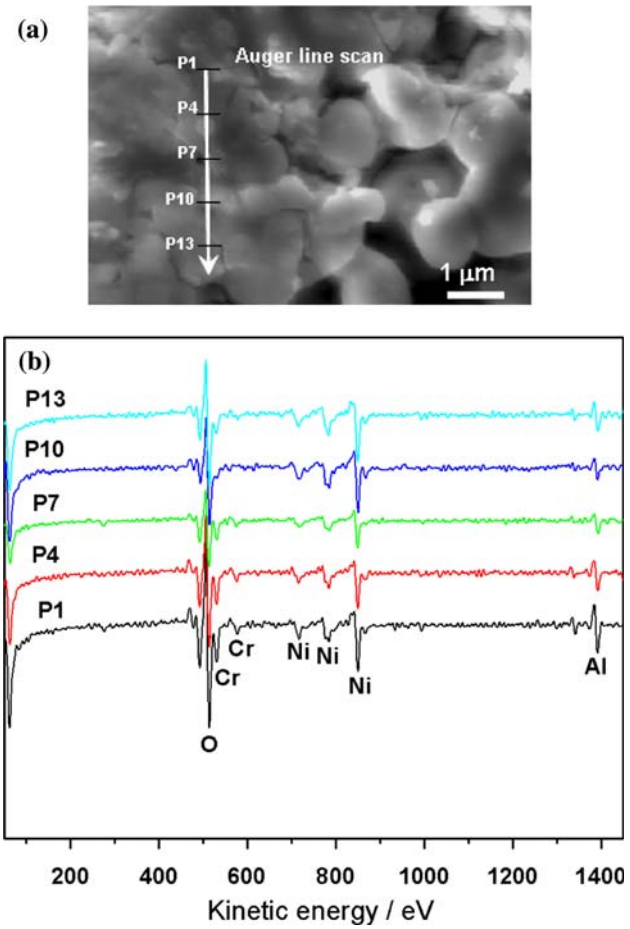

Fig. 6 SEM images and local Auger spectra at various points marked on the SEM image for Ni–Al–Cr_3 catalyst after leaching in NaOH. Cr concentration: P1—11 at.%, P4—13 at.%, P7—14 at.%, P10—0 at.%, P13—3 at.%

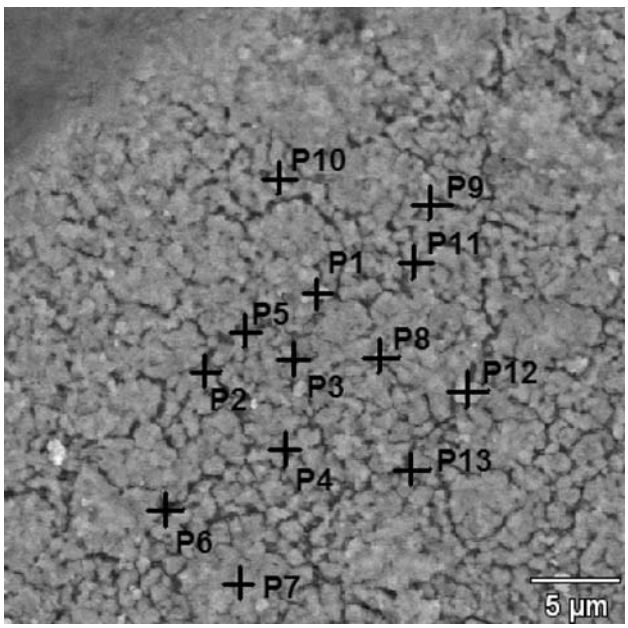

Fig. 7 SEM image of Ni–Al–Cr catalyst with marked points of local EDS analysis

Table 3 Results of local EDS analysis of Ni–Al–Cr_3 catalyst after full leaching at points from P1 to P13 (see Fig. 7)

	O–$K\alpha$	Al–$K\alpha$	Cr–$K\alpha$	Ni–$K\alpha$
p1	12.9	11.1	1.3	74.7
p2	6.3	8.7	1.0	84.0
p3	15.0	8.7	2.1	74.2
p4	24.8	9.2	2.7	63.3
p5	28.7	8.3	6.2	56.8
p6	21.1	4.2	6.8	67.9
p7	6.6	6.6	1.6	85.2
p8	16.3	12.3	1.8	69.6
p9	20.4	7.1	1.6	70.9
p10	9.0	11.0	1.5	78.5
p11	25.0	8.4	5.1	61.5
p12	18.7	7.2	3.1	71.0
p13	18.1	7.1	2.9	71.9

Data are given in at.%

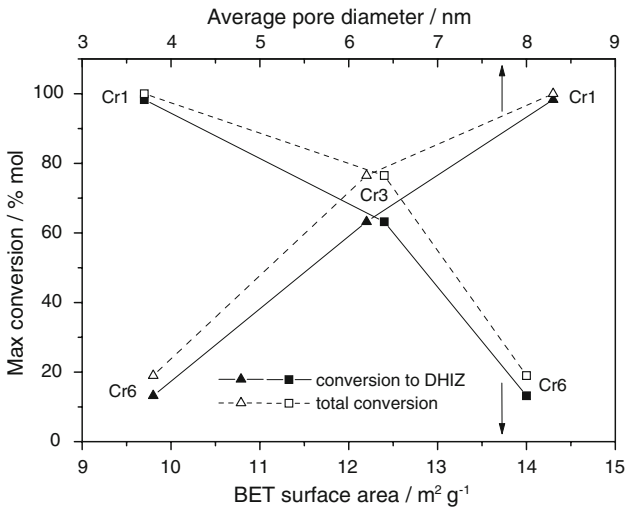

Fig. 8 Conversion to dihydroisophorone versus BET surface area and averaged pore diameter for Ni–Al–Cr catalysts containing initially 1, 3, and 6 at.% Cr

surface area seem to be more important for the catalytic activity and selectivity of the alloys studied.

An attempt was made to explain the effect of Cr by its influence on the electron band structure of Ni near the Fermi level [36] (a suggestion was made that Cr doping may thus be favorable for hydrogen adsorption on Ni–Al–Cr catalyst, and so may also modify the catalytic properties of Ni [36]). According to Friedel [37] metallic nickel doped with 3d metals like Cr (even at small concentration) exhibits dramatic change of electronic band structure (concerning itinerant electrons) due to formation of virtual bound states (VBS) near the Fermi level [38, 39]. Due to the presence of VBS near the Fermi level, there are more empty states available in Cr-doped Ni comparing to pure Ni. This modification of electronic structure may enhance catalytic properties of the nickel matrix. However, although Co does not exhibit such an influence, Co doping of Raney Ni catalyst also improvers selectivity [40]. Therefore, this behavior cannot be solely ascribed to the differences in electronic structure of these materials and other factors, most likely surface chemistry, should also be considered [40].

The surface analytical (AES, SAM) and microanalytical (EDS) results [36, 40] suggest that the enrichment of minor components (Cr, Co) and specific morphology promote the modification of catalytically active Ni sites on the surface of Ni-Raney type alloys, so that they become highly selective for C=C bond hydrogenation in isophorone. Due to Cr or Co enrichment, the active hydrogenation sites (an ensemble of a few Ni atoms) may become very small and able to chemisorb the C=C bond only, and not the C=O bond. The decrease in hydrogenation activity with Cr or Co content is in agreement with the smaller size of the chemisorption sites, and may suggest a decrease in Ni surface area.

Another factor, which may largely contribute to selectivity is the presence of oxygen in areas enriched in Cr (or Co), as suggested by XPS investigations (Cr and Co are oxidized, whereas Ni seems to remain unoxidized, see Fig. 4 in Ref. [40]). Hence, the presence of $O^{\delta-}$, Cr^{ox} (or $O^{\delta-}$ and Co^{ox}) entities within an active center may tend to repel the C=O tail of an isophorone molecule, and, at the same time, enhance hydrogenation of the C=C bond by promoting the suitable arrangement of N···H surface complexes in the near vicinity. For NiAlCr alloy catalysts, the active center should contain the following entities: $O^{\delta-}$, Cr^{ox}, and Ni, as shown in Fig. 9. In this sense, the role of $O^{\delta-}$, Cr^{ox} (or $O^{\delta-}$ and Co^{ox}) entities would be to restrain hydrogenation of the C=O group in isophorone.

Dehydrogenation of 2-propanol on modified Cu–Hf catalysts

The dehydrogenation of aliphatic alcohols to produce the corresponding carbonyl compounds is one of the reactions requiring an efficient catalyst to proceed. Cu powder is

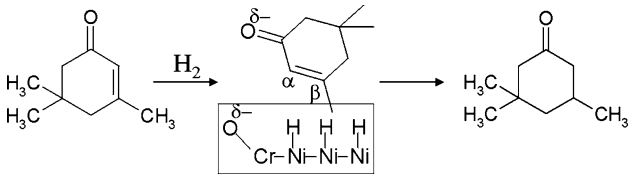

Fig. 9 Tentative mechanism of hydrogenation of isophorone on Ni–Al–Cr catalyst. An active center consists of $O^{\delta-}$, Cr^{ox}, entities and N···H surface complexes

known to catalyze such processes, but easily becomes deactivated, mostly due to sintering. In order to improve performance, supported Cu catalysts, usually Cu on an oxide support, are used. The best examples of these are the binary and ternary industrial Cu–metal oxide systems used in methanol synthesis [41–43]. Recent investigations have shown, however, that Cu–Hf and Cu–Ti amorphous alloys are precursors of catalysts exhibiting excellent selectivity in the dehydrogenation of aliphatic alcohols [16, 44].

Cu65–Hf35 amorphous alloy ribbons (4 mm wide, 40 μm thick) were used. The ribbon was produced by continuous casting from a melt on a rotating copper wheel in an inert atmosphere of pure nitrogen. Amorphous samples were hydrogen charged to increase their catalytic activity for the dehydrogenation of 2-propanol. Cathodic charging at 25 °C in 0.1 M H_2SO_4 at a constant current density was applied during time intervals from 24 h up to 100 h. Low current density (usually -1 mA/cm^2) and prolonged controlled charging time were applied to produce subtle effects.

Hydride formation during cathodic hydrogen charging was the most probable event there as group IVA metals are known for their tendency to readily form hydrides [17, 44, 45]. Apparently, Hf hydride formation is only an intermediate step, forcing Cu to migrate to the surface and segregate. Then, the hydride decomposes at room temperature and Hf undergoes oxidation. Figure 10 summarizes the effect of cathodic hydrogen charging on the geometrical parameters of the surface of Cu–Hf catalyst (BET surface area and porosity estimated for the total weight of the ribbon). Although BET areas are not necessarily relevant to catalysis, the rather small values (a few meters squared per gram) are indicative of a small concentration of active sites. It is noteworthy that for Cu–Hf, both the BET surface area and porosity grow with hydrogen charging time.

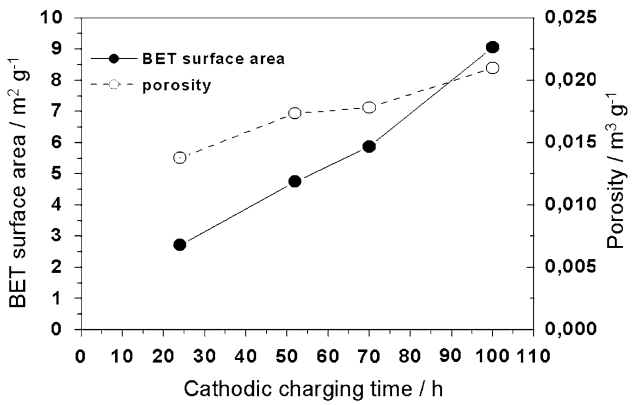

Fig. 10 Effect of cathodic hydrogen charging on BET surface area and porosity of Cu–Hf catalyst

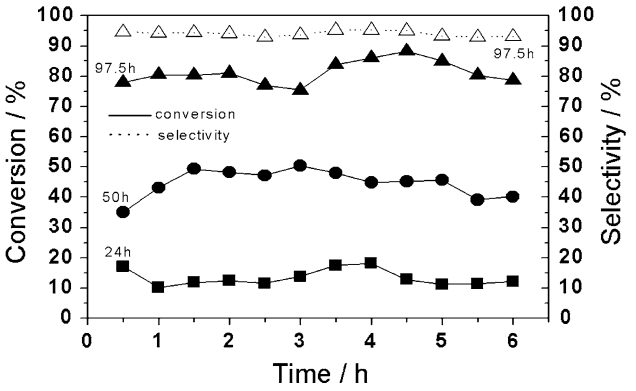

Fig. 11 Catalytic activity and selectivity of Cu–Hf samples versus time of catalytic test after hydrogen charging pretreatment from 24 to 97.5 h, as indicated

Figure 11 shows the catalytic activity and selectivity of Cu–Hf samples after hydrogen charging from 24 to 97.5 h. A stable catalytic activity of about 80% was detected with an *excellent selectivity to acetone formation of 95%*. This result is of particular interest and significance as it was obtained at a BET surface area of several square meters per gram (compare Fig. 10). The corresponding catalytic efficiencies estimated for the BET surface area (average) for Cu65–Hf35 alloy hydrogen charged for 100 h is 0.4×10^{-2} mol/m^2 h [44].

It is clear that the catalytic activity of Cu–Hf increases with hydrogen charging time because of the development of surface area and porosity. Moreover, earlier Raman investigations suggested, that partial devitrification of Cu–Hf produced different kinds of adsorption active sites on the surface [46]. In the test reaction, catalytic activity was stable for 6 h and for longer periods. Catalysts produced from the amorphous precursors were durable and did not undergo any deactivation.

Subtle chemical and morphological changes in Cu–Hf alloy introduced by hydrogen charging were examined by SEM and high-resolution SAM techniques. Examinations of the hydrogen-treated samples with a high-resolution scanning microscope and scanning Auger confirmed that the surface developed, mostly due to Cu segregation, upon cathodic hydrogen charging (Fig. 12). Well-developed particles and their agglomerates are present on the surface. Local Auger spectra shown in Fig. 12 (P1 and P2) reveal that the clusters are of pure Cu. Copper is probably slightly oxidized, as O (510 eV) signal is well distinguishable in the spectrum. The substrate, on the other hand, is strongly oxidized Hf. These results coincide with that found for Cu–Hf amorphous alloy aged in air [16], that is, the samples consist of Cu particles supported on HfO_2.

As already mentioned, Hf hydride formation has forced Cu to migrate up to the surface and segregate. Then, the

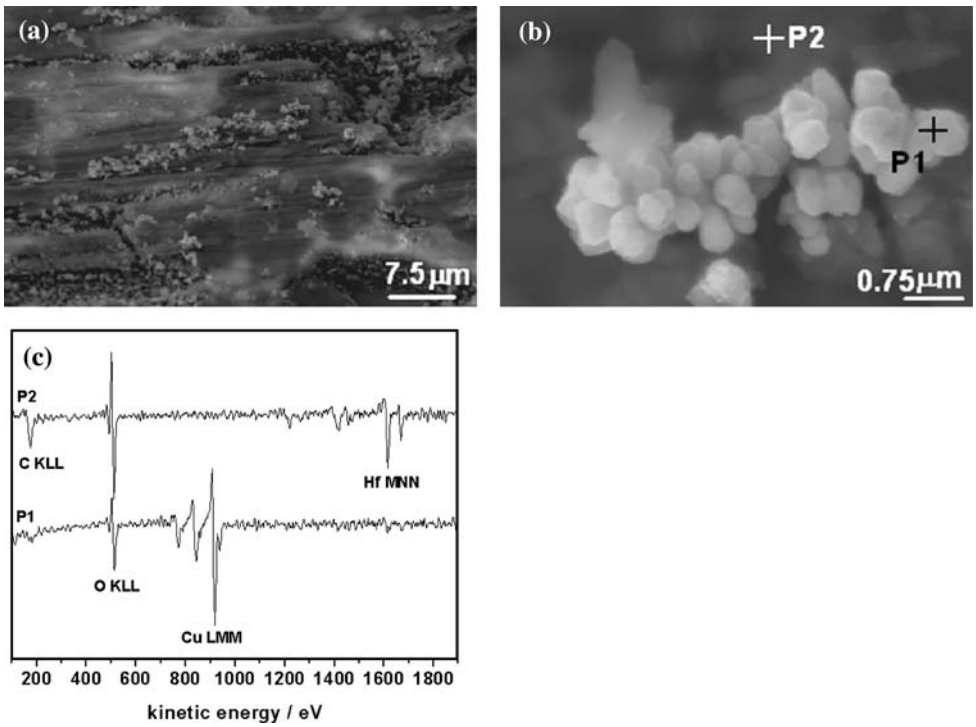

Fig. 12 SEM images and Auger spectra recorded at points marked for Cu–Hf catalyst after hydrogen charging

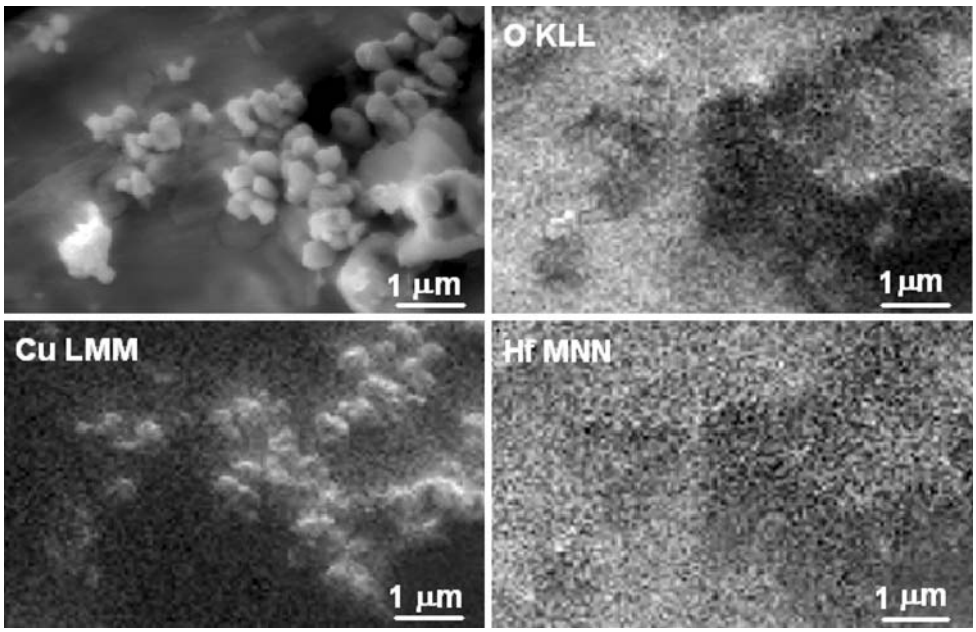

Fig. 13 SEM image (**a**) and distribution images of elements: Hf (**b**), Cu (**c**), and O (**d**) on Cu–Hf catalyst, after 97.5 h hydrogen charging

hydride decomposed, Hf underwent oxidation. No Cu signal is visible there suggesting that HfO_2 layer is sufficiently thick to quench Cu signals from the amorphous material underneath.

Figure 13 shows high-resolution Auger maps for Cu65–Hf35 amorphous alloy after hydrogen charging at $i = -1$ mA/cm^2 in 0.1 M H_2SO_4 for 97.5 h. The SAM maps of the surface show Cu-rich particles, with HfO_x-rich area underneath (the areas enriched in Hf coincide with those enriched in oxygen). These results indicate a full separation of the two elements (Cu and Hf) as a result of a devitrification process within the surface layer.

Figure 14 shows a scheme of dehydrogenation of 2-propanol to acetone on a partially oxidized copper catalyst [47, 48]. The mechanism involves Cu^0, $Cu^{\delta+}$, and $O^{\delta-}$ entities forming an active center. This mechanism is also valid for the reaction on a Cu/HfO_2 catalyst prepared from Cu–Hf amorphous precursors.

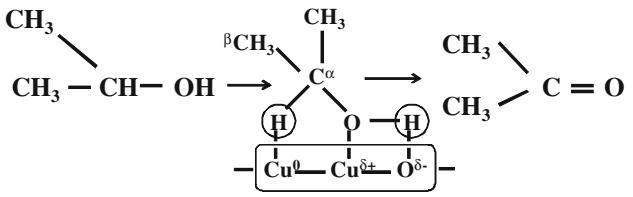

Fig. 14 Tentative mechanism of dehydrogenation of 2-propanol on Cu powder and on Cu/HfO_2 catalyst made from a Cu–Hf amorphous precursor

It should be pointed out, however, that the above mechanism is *not valid* for the selective dehydrogenation of 2-propanol on a *catalyst prepared from Cu–Ti amorphous precursor* because a more complex morphology and chemistry of the catalyst is developed due to hydrogenation. Therefore, a new mechanism was proposed; details are given elsewhere [16].

Concluding remarks

In this review, we discuss several examples of investigations on the preparation and characterization of metal alloy catalysts fabricated from rapidly quenched precursors for hydrogenation and dehydrogenation of organic compounds or steam reforming of methanol. In the former context Ni-based catalysts were explored, while in the latter one Cu- or Pd-based alloys were studied. In particular, using high-resolution local characterization techniques of SEM and AES, an insight into the mechanism of catalytic action of the materials studied was gained. The local chemical and morphological changes of the catalyst at the micro- and nanometer scale during modification of the catalyst precursor could be monitored. In recent work, an attempt was made to find an interrelation between the composition, structure, and morphology of catalysts and their activity and selectivity in the catalytic processes investigated [49]. The examples discussed above illustrate the role of high-resolution methods in characterizing local differences in the chemistry of catalytic materials. They also visualize various possibilities of modifying the properties of metastable amorphous and nanostructured materials by chemical or electrochemical degradation processes, which—being generally detrimental—are in those particular cases beneficial in enhancing catalytic properties of certain alloys.

Acknowledgements We are most grateful to Prof. Árpad Molnár and to all the co-authors who contributed their knowledge and experience to the joint papers quoted in this review. This work was financially supported by the Polish Ministry of Education and Science through grant N507 133 32/3949. Surface characterizations were performed using a Microlab 350 located at the Physical Chemistry of Materials Center of the Institute of Physical Chemistry, PAS and of the Faculty of Materials Science and Engineering, WUT.

References

1. Ertl G, Knözinger H, Weitkamp J (1999) Environmental catalysis. Wiley-VCH, Weinheim
2. Hashimoto K (1997) Mat Sci Eng A Struct 226–228:891
3. Libuda J, Schauermann S, Laurin M, Schalow T, Freund H-J (2005) Monatshefte Chem 136:59
4. St Clair TP, Goodman DW (2000) Top Catal 13:5
5. Freund H-J, Kuhlenbeck H, Libuda J, Rupprechter G, Bäumer M, Hamann H (2001) Top Catal 15:201
6. Freund H-J (2008) Top Catal 48:137
7. Molnár Á, Smith GV, Bartók M (1989) Adv Catal 36:329
8. Baiker A, Molnár Á (2008) In: Ertl G, Knözinger H, Weitkamp J (eds) Handbook of heterogeneous catalysis, 2nd edn, vol 3, chap 4.4. Wiley-VCH, Weinheim, p 1285
9. Mäki-Arvela P, Hájek J, Salmi T, Murzin DYu (2005) Appl Catal A 292:1
10. Somorjai GA, Yang M (2003) Top Catal 24:61
11. Greer AL (1997) Curr Opin Solid State Mater Sci 2:412
12. Molnár A, Domokos L, Martinek T, Katona T, Mulas G, Cocco G, Bertóti I, Szépvölgyi J (1997) Mater Sci Eng A 226–228:1074
13. Deng J-F, Li H, Wang W (1999) Catal Today 51:113
14. Nowakowski R, Seidel C, Fuchs H (2004) Surf Sci 562:53
15. Løvvik OM, Opalka SM (2008) Surf Sci 602:2840
16. Pisarek M, Janik-Czachor M, Molnar A, Hughes K (2005) Appl Catal A 283:177
17. Pisarek M, Janik-Czachor M, Molnar A, Rac B (2005) Electrochim Acta 50:5111
18. Janik-Czachor M, Szummer A, Bukowska J, Molnar A, Mack P, Filipek SM, Kędzierzawski, Kudelski A, Pisarek M, Dolata M, Varga M (2002) Appl Catal A 235:157
19. Zhang HF, Wang AM, Li H, Song QH, Ding BZ, Hu ZQ (2001) Mater Lett 48:347
20. Takahashi T, Inoue M, Kai T (2001) Appl Catal A 218:189
21. Iwasa N, Masuda S, Ogawa N, Takezawa N (1995) Appl Catal 125:145
22. Inui T, Suehiro M, Takegami Y (1982) J Petrol Inst 25:63
23. Takahashi K, Takahashi H, Akazawa T, Takezawa N, Kobayashi H (1984) Shokubai 26:318
24. Kudelski A, Pettinger B (2004) Surf Sci 566–568:1007
25. Li H, Wang W, Zong B, Min E, Deng J-F (1998) Chem Lett 27:371
26. Li H, Xu Y, Deng J-F (1999) New J Chem 23:1059
27. Li H, Wang W, Li H, Deng J-F (2000) J Catal 194:211
28. Li H, Li H, Dai W-L, Wang W, Fang Z, Deng J-F (1999) Appl Surf Sci 152:25
29. Molnár Á, Sárkány A, Varga M (2001) J Mol Catal A 173:185
30. Varga M, Molnár A, Mohai M, Bertóti I, Janik-Czachor M, Szummer A (2002) Appl Catal A 234:167
31. Katona T, Molnar A (1995) J Catal 153:333
32. Guczi L, Schay Z, Stefler Gy, Liotta LF, Deganello G, Venezia AM (1999) J Catal 182:456
33. Gallezot P, Richard D (1998) Catal Rev Sci Eng 40:81
34. Kijeński J, Winiarek P (2000) Appl Catal A 193:L1
35. Kijeński J, Winiarek P, Paryjczak T, Lewicki A, Mikołajska A (2002) Appl Catal A 233:171
36. Pisarek M, Łukaszewski M, Winiarek P, Kędzierzawski P, Janik-Czachor M (2008) Catal Commun 10:213
37. Friedel J (1962) J Phys Rad 23:692
38. Filipek SM (1989) Z Phys Chem N F 163:627
39. Filipek SM (1989) Z Phys Chem N F 163:485
40. Pisarek M, Łukaszewski M, Winiarek P, Kędzierzawski P, Janik-Czachor M (2009) Appl Catal A 358:240
41. Kung HH (1980) Catal Rev Sci Eng 22:235
42. Klier K (1982) Adv Catal 31:243

43. Bart JCJ, Sneeden RPA (1987) Catal Today 2:1
44. Pisarek M, Janik-Czachor M (2006) Microsc Microanal 12:228
45. Fromm E, Gebhardt E (1976) Gase und Kohlenstoff in Metallen. Springer, Berlin, pp 406–416
46. Kudelski A, Janik-Czachor M, Bukowska J, Pisarek M, Szummer A (2002) Mat Sci Eng A 326:364
47. Madix RJ (1980) Adv Catal 29:1
48. Chung M-J, Han S-H, Park K-Y, Ihm S-K (1993) J Mol Catal 79:335
49. Pisarek M, Łukaszewski M, Janik-Czachor M (2009) Pol J Chem 83:1393